applied sciences

MDPI

Article

Terahertz Absorption Spectroscopy in Bicrystal Josephson Junctions Formed from Mutually Tilted *c*-Axes $YBa_2Cu_3O_{7-x}$ Films

Yuriy Divin

Kotelnikov Institute of Radioengineering and Electronics, Russian Academy of Sciences, 125009 Moscow, Russia; yyd@cplire.ru

Abstract: Spectral analysis of terahertz (THz) and sub-THz emission from quantum cascade lasers has been recently demonstrated using conventional $YBa_2Cu_3O_{7-x}$ bicrystal Josephson junctions made from *c*-axes thin films. Josephson frequencies of alternative bicrystal junctions made from $YBa_2Cu_3O_{7-x}$ films with mutually tilted c-axes extend further into the THz range. However, these THz oscillations can weaken due to new absorption channels in the junction environment. Here, using Josephson admittance spectroscopy, THz losses in $YBa_2Cu_3O_{7-x}$ bicrystal junctions with mutually tilted *c*-axes are studied. Absorption maximizes at a reproducible set of THz frequencies close to those of collective modes in bulk $YBa_2Cu_3O_{7-x}$ recovered by Fourier spectroscopy. Annealing junctions in atomic oxygen reduces the losses at frequencies of 2.7 and 3.6 THz, while the losses increase at frequencies of 2.3 and 4.6 THz. Thus, as a THz spectrum analyzer, $YBa_2Cu_3O_{7-x}$ bicrystal junctions require post-fabrication correction of the oxygen content. In addition, the fine structure of the absorption spectrum appears at frequencies near 4.6 THz. Significant absorption near 2.3 THz may be due to effects associated with the second Josephson harmonic or second-order nonlinearity of the susceptibility in $YBa_2Cu_3O_{7-x}$. This work paves the way towards probing collective modes in high-T_c materials in situ using the Josephson oscillations.

Keywords: Josephson junctions; spectroscopy; terahertz; high-temperature superconductors; absorption

Citation: Divin, Y. Terahertz Absorption Spectroscopy in Bicrystal Josephson Junctions Formed from Mutually Tilted *c*-Axes $YBa_2Cu_3O_{7-x}$ Films. *Appl. Sci.* **2023**, *13*, 5766. https://doi.org/10.3390/app13095766

Academic Editor: Mira Naftaly

Received: 31 March 2023
Revised: 3 May 2023
Accepted: 5 May 2023
Published: 7 May 2023

1. Introduction

With the discovery of high-temperature (high-T_c) superconductivity [1], it became possible, in principle, to fabricate Josephson junctions (JJs) [2] with higher Josephson frequencies f_j than those of low-T_c superconductor junctions. Due to small coherence lengths, even grain boundaries in high-T_c materials have the properties of weak links and JJs [3]. The most common high-T_c junctions are artificial bicrystal JJs formed by the coalescence of two misoriented high-T_c films [3]. The bicrystal junction consists of a structurally distorted interface in the middle and two adjacent layers of undistorted material with a reduced oxygen content and, accordingly, a depleted charge region [3]. Such a boundary is a potential barrier for the tunneling Cooper pairs and quasiparticles.

Conventional bicrystal JJs are fabricated from two *c*-axes high-T_c films. They have characteristic voltages I_cR_n up to 3 mV, which is significantly lower than the gap voltages $2\Delta/e$ for high-T_c materials. In these junctions, the dependence of the supercurrent I_s on the phase difference φ of the order parameters turned out to be close to sinusoidal, as in classical tunnel JJs. Moreover, the dynamics of such JJs is close to a simple resistively shunted junction (RSJ) model, where, along with the supercurrent $I_s = I_c\mathrm{Sin}\varphi$, the quasiparticle current enters into the total current in the form of Ohm's law: $I_q = V/R_n = (\hbar/2eR_n)(\mathrm{d}\varphi/\mathrm{d}t)$ [4]. These circumstances played an important role when using JJs as frequency-selective detectors and served as a stimulus for intensive studies of spectroscopic applications of high-T_c JJs in a broad spectral range (see, for example, [5]).

The further development of these works has already made possible several spectroscopic applications of high-T_c JJs. Among them are the following: the identification

of liquids by their sub-THz reflection [6], the detection of broadband radiation from quasiparticle-injected nonequilibrium superconductors [7] and photoconductive antennas excited by femtosecond optical pulses [8], and the detection of 500 GHz radiation from a $Bi_2Sr_2CaCu_2O_8$ intrinsic Josephson junction [9]. In high-energy physics, it was possible to substantiate and partially implement high-T_c JJs for spectral analysis of transition radiation from relativistic electron bunches in linear accelerators [10] and cyclotron electron emission from high-temperature plasma in tokamaks [11]. Previous studies of output sub-THz and THz radiation from commercial sources [12–16] with high-T_c JJs have paved the way for the spectral characterization of new THz sources based on quantum cascade lasers (QCLs) [17,18]. Recently, using high-T_c JJs, subterahertz spectral lines have been found in the emission of free-running THz quantum cascade lasers (QCLs) due to difference-frequency generation (DFG) in the QCL active region [19].

Application of high-T_c JJs for the characterization of QCLs radiation looks very promising and competitive because these spectral measurements are in the frequency domain [18] and possess the potential to operate both in the sub-THz and THz ranges [17–19]. The latter circumstance is for verification in various configurations of high-T_c JJs with proper tuning of relevant parameters of the junctions. Previously, Josephson bicrystal junctions, consisting of two c-oriented $YBa_2Cu_3O_{7-x}$ thin-film electrodes, were mainly used for spectroscopic purposes [5–19]. The simple bicrystal junction, where the *c*-axis epitaxial films grow on each part of the bicrystal substrate, forms an artificial bicrystal boundary by the coalescence of two misoriented *c*-axis thin-film parts. This boundary in $YBa_2Cu_3O_{7-x}$ thin-film acts as a potential barrier for tunneling Cooper pairs and quasiparticles. However, due to the island growth of the *c*-axis $YBa_2Cu_3O_{7-x}$ films, such a bicrystal boundary has a variety of facets with various local misorientations that give rise to an inhomogeneous current distribution [3,20].

It is advantageous to use the bicrystal junctions formed by two $YBa_2Cu_3O_{7-x}$ thin-film electrodes with mutually tilted *c*-axes, which leads to more homogeneous current distributions, lower specific resistances R_nA and higher characteristic voltages I_cR_n of $7 \div 8$ mV [21,22]. This combination of the electrical parameters of the JJs can result in lower Josephson linewidths $\delta f \sim R_n$, higher amplitudes of Josephson oscillations $V_1 \sim I_cR_n$, and characteristic Josephson frequencies $f_c = 2eI_cR_n/h$. However, it should be taken into account that these Josephson frequencies, although far from the gap frequencies, are close to the frequencies f_k of optical phonons in high-T_c thin-film electrodes. The amplitudes of Josephson oscillations at the frequencies $f_j \approx f_k$ can weaken due to strong absorption by optical phonons. A negative consequence of this interaction is that a spectrum analyzer using Josephson junctions with high-I_cR_n products will be blind near the phonon frequencies f_k. Thus, to find the spectral range of continuous operation of the Josephson spectrum analyzer, one should study the absorption spectra in JJs in situ. In this paper, we use the approach that interaction between Josephson oscillations and optical phonons is accompanied by a localized modification of the dc *I*–*V* curves of JJs around the voltages $V_k = hf_k/2e$ and the absorption spectra in JJs can be recovered from their dc *I*–*V* curves.

Additional arguments stimulating our study of the interaction of Josephson oscillations with the high-T_c electrodes come from the current state of far-infrared reflection spectroscopy of collective modes in high-T_c materials [23–30]. Some difficulties in measuring low-frequency dynamic conductivities due to the high reflectivity of the samples when the electric field *E* is parallel to the ab-planes and due to diffraction effects at frequencies below 150 cm^{-1} (4.5 THz) have been reported [25,29]. Josephson spectroscopy applied in situ to high-T_c materials can be free from these limitations and give additional information on low-frequency collective modes in the electrode materials.

In this paper, the results of the study of $YBa_2Cu_3O_{7-x}$ bicrystal junctions with mutually tilted *c*-axes concerning their possible applications in terahertz Josephson spectroscopies are presented.

2. Junctions and Methods

2.1. Junctions

We used the valley type of bicrystal high-T_c JJs with mutually tilted *c*-axes [21] schematically shown in Figure 1a. Each high-T_c electrode looks like a stack of superconducting layers along the *a*-*b* planes. Thin-film electrodes to the left and the right of the bicrystal boundary (plane $x = 0$) have the c-axes tilted toward the boundary by the same angle α, and the *a*-axes are parallel to the boundary. Previously, there were attempts to assume that the *a*- or *b*-axis passes along the bicrystal boundary and to consider films with a tilt of the *c*-axis due to rotation around the [100]- or [010]-axis, respectively. However, our $YBa_2Cu_3O_{7-x}$ thin films consist of twin domains with a set of twin boundaries, where the *a*- and *b*-orientations of the film change directions. Therefore, we call such junctions "bicrystal junctions with mutually tilted *c*-axes." Because of twinning in the junction electrodes, it can be expected that a high-frequency electromagnetic electric field generated perpendicular to the bicrystal boundary can excite collective modes in the electrodes both in *a*- and *b*-directions. The same remark is also valid for the mode excitation along the *c*-axis.

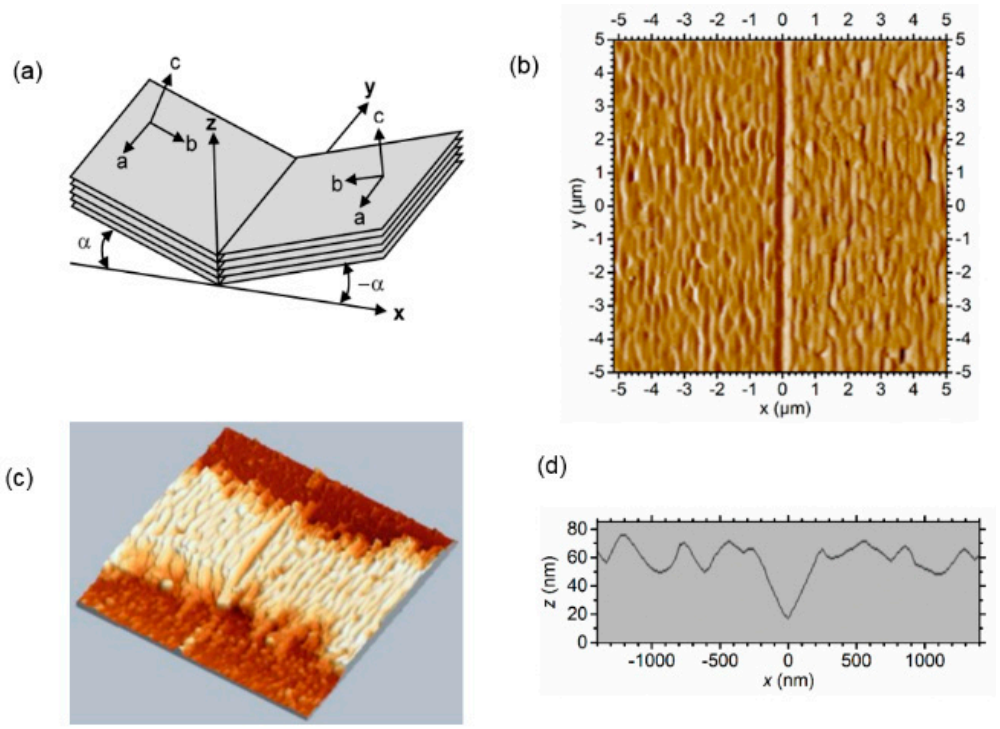

Figure 1. (**a**) Schematic representation of a bicrystal high-T_c junction of the "valley" type with mutually tilted *c*-axes. (**b**) AFM amplitude image (10×10 μm^2) of a typical fabricated $YBa_2Cu_3O_{7-x}$ thin film on a $2 \times 12°$ $SrTiO_3$ bicrystal substrate consisting of two parts with mutually tilted *c*-axes. Sample yd107201. (**c**) AFM topographic image (9×9 μm^2) of an $YBa_2Cu_3O_{7-x}$ thin-film bridge across the bicrystal boundary on a $SrTiO_3$ bicrystal substrate with mutually tilted *c*-axes. Sample yd107111. (**d**) Profile of the film surface during scanning across the bicrystal boundary. The plane z = 0 is the plane of the substrate.

Valley-type JJs were fabricated by epitaxial growth of $YBa_2Cu_3O_{7-x}$ thin films on bicrystal substrates made from $NdGaO_3$, $SrTiO_3$ or $NdGaO_3$ with a thin (≈10 nm) buffer layer of $SrTiO_3$. The bicrystal parts of the substrates were oriented to get the mutual tilt of the *c*-axes of the counter electrodes [20,21]. For the deposition of thin films, we used dc sputtering from a stoichiometric target at a high oxygen pressure of 3.0–3.4 mbar and heater temperatures of 930°C – 970°C. The deposition rate was about 1 nm per minute. After deposition, the films were at an oxygen pressure of 1 bar and a heater temperature of 550°C for 30 min. Figure 1b shows the AFM amplitude image for a typical $YBa_2Cu_3O_{7-x}$ thin film

fabricated on a bicrystal $SrTiO_3$ substrate with the *c*-axes tilted to the boundary by ±12°. The film regions remote from the bicrystal boundary (x = 0) consist of grains extended up to 1–2 μm in the y-direction along the boundary and compressed to approximately 0.2 μm in the x-direction perpendicular to the boundary.

In the region of the bicrystal boundary, the deposited thin $YBa_2Cu_3O_{7-x}$ film has a regular V-shaped profile, which is the result of the nucleation of $YBa_2Cu_3O_{7-x}$ at the boundary of the substrate bicrystal (x = 0) and the predominant growth of $YBa_2Cu_3O_{7-x}$ along the *a*-*b* plane in the left and right parts of the bicrystal substrates. The bicrystal boundary in a thin film here deviates from the substrate boundary by no more than ±20 nm, which is approximately an order of magnitude less than the meandering of grain boundaries in conventional bicrystal JJs made from *c*-oriented films. Figure 1b shows only the topography of the film surface, and a substrate level is required to obtain a cross-section.

We fabricated thin-film bridges across the bicrystal interface using PMMA-based UV lithography and etching in 0.1% Br/ethanol. Figure 1c shows a topographic image AFM of a 5 μm wide $YBa_2Cu_3O_{7-x}$ bridge fabricated across the bicrystal boundary on a $SrTiO_3$ substrate. The combination of two profiles of a thin-film bridge, measured across the bicrystal boundary in the middle of the bridge and the bridge outside the bicrystal boundary, gives the cross-section $z(x)$ in Figure 1d, where the level z = 0 is the substrate surface. The V-shaped surface profile of $YBa_2Cu_3O_{7-x}$ near the bicrystal boundary has slopes at an angle of ±12° to the substrate surface. Growth islands in both electrodes form terraces with a step height of 5 ÷ 20 nm. One can see from Figure 1d that the average thickness of the $YBa_2Cu_3O_{7-x}$ thin film, except for the bicrystal boundary, is (65 ± 10) nm, and the film thickness at the boundary is about 20 nm.

To increase the oxygen content in JJs after fabrication, these JJs were annealed in an ozone/oxygen mixture at 1 bar under UV irradiation at a temperature of 140 °C for 30 min [31]. The junction resistances R_n decrease approximately twice after this annealing, while the critical temperature T_{c0} of 87.5 K remains. Such low-temperature annealing can initiate diffusion of atomic oxygen through the bicrystal boundary but increases only the concentration of oxygen atoms in the Cu-O chains of $YBa_2Cu_3O_{7-x}$ electrodes [32]. Thus, the collective modes containing oxygen in the chains in the $YBa_2Cu_3O_{7-x}$ adjacent to the boundary are under selective doping. The interaction of Josephson oscillations with these modes in $YBa_2Cu_3O_{7-x}$ electrodes reflects on the *I*–*V* curve, and Josephson admittance spectroscopy [33] can describe this modification.

2.2. Josephson Admittance Spectroscopy

The dc current-voltage dependence, $I_0(V)$, of an autonomous JJ is the result of averaging the Josephson oscillations and has the following form in the RSJ model [4]:

$$I_0(V) = Sign(V)R_n^{-1}\left(I_c^2R_n^2 + V^2\right)^{1/2} \quad (1)$$

where I_c is the critical current, and R_n is the normal-state resistance of JJ. The deviation of this *I*–*V* curve (Equation (1)) from the *I*–*V* curve of the JJ in the normal state, $I_q(V) = V/R_n$, is due to the time averaging of Josephson voltage oscillations $V(t)$ with an amplitude of $2I_cR_n$ and the Josephson frequency $f_j = 2eV/h$.

An autonomous RSJ-like Josephson junction with the *I*–*V* curve described by Equation (1) is an idealization. In our case, the high-T_c thin-film JJ is located on a dielectric substrate, and high-T_c thin-film electrodes are attached to the JJ for dc biasing and voltage measurement. Here, the dielectric and high-T_c materials are of finite dimensions and have their dynamic conductivities $\sigma(f)$. The total effect of such an electromagnetic environment on JJ is usually described by introducing an external admittance $Y_e(f)$ connected to the RSJ-like JJ. The real part of the $Y_e(f)$ can be determined directly from the *I*–*V* curve of JJ according to Josephson admittance spectroscopy [33]. To find a contribution to the admittance $Y_e(f)$ from the collective modes in dynamic conductance $\sigma(f)$ of high-T_c electrodes, a set of $Y_e(f)$-measurements, where the substrates are changed, should be compared, and the study

should be focused on the features, which are not changed. Additional low-temperature oxygen loading can affect only the collective modes in high-T_c materials and thus reveal these modes.

When an external admittance $Y_e(f)$ shunts the JJ, the dynamics of the Josephson oscillations change compared to those of the autonomous JJ, and the dc *I–V* curve changes accordingly. One should highlight that the reactive, by an inductance L or a capacitance C, shunting of the JJ led to a modification of the JJ dynamics, which for low total conductivities Y_L and Y_C has only a quadratic effect on the dc *I–V* curve proportional to ${Y_L}^2$ or ${Y_C}^2$ [34]. However, for an arbitrary external admittance $Y_e(f)$ of small values $|Y_e(f_c)| << {R_n}^{-1}$, the modification of the dc *I–V* curve depends linearly on the real part of the conductivity Y_e, namely [33],

$$\Delta I(V) = -V\left[1 - \frac{V}{(I_c^2 R_n^2 + V^2)^{\frac{1}{2}}}\right] \mathrm{Re}Y_e(2eV/h) \quad (2)$$

where $\Delta I(V) = I_e(V) - I_0(V)$ is the difference between the *I–V* curve perturbed by the external conductance $Y_e(f)$ and the autonomous *I–V* curve of the RSJ type according to Equation (1), $Y_e(0) = 0$. Thus, it is possible to obtain the spectral distribution of losses in an external admittance connected to the JJ from the change in the experimental *I–V* curves using Equation (2). The voltage-dependent factor relating $\Delta I(V)$ and $\mathrm{Re}Y_e(f)$ has a maximum of $0.3I_cR_n$ at the voltage around $0.8I_cR_n$. The characteristic voltage I_cR_n determines the spectral range and sensitivity of Josephson admittance spectroscopy.

Figure 2 shows how the *I–V* curve changes with a hypothetical external admittance $Y_e(f)$. The presence of two weak absorption lines in $\mathrm{Re}Y_e(f)$ at dimensionless frequencies $f_1/f_c = 0.75$ and $f_2/f_c = 2.0$ (bottom panel) leads to the corresponding two dips in the dc *I–V* curve at dimensionless voltages $V/I_cR_n = 0.75$ and 2.0 (top panel). The difference between the *I–V* curve (I_e, blue curve) of the JJ under shunting by the admittance $Y_e(f)$ and the autonomous curve (I_0, dashed grey curve) is small and localized at the voltages $V_{1,2} \approx \mathrm{h}f_{1,2}/2\mathrm{e}$ (see Figure 2). It is advisable to measure the derivatives of the *I–V* characteristics to improve the signal/noise ratio, as in other types of tunneling spectroscopy [35]. Indeed, the differential conductance $\mathrm{d}I/\mathrm{d}V$ vs. V (a dark cyan line) demonstrates two odd-symmetric features of extended amplitudes but the effect of the external admittance on the *I–V* curve is considerably smaller.

To recover the $\mathrm{Re}Y_e(f)$ from the measured differential conductances $\mathrm{d}I/\mathrm{d}V$ vs. V, one needs to integrate the difference between the derivative $\mathrm{d}I/\mathrm{d}V$ modified by the external conductivity (a green curve on the top panel of Figure 2) and the derivative $\mathrm{d}I_0/\mathrm{d}V$ for the autonomous JJ (a grey dashed line on the top panel of Figure 2), get the difference $\Delta I(V)$ + C with some constant C of integration, which is determined by comparison with the difference between the *I–V* curve measured with the external admittance and the *I–V* curve according to Equation (1), and finally, calculate $\mathrm{Re}Y_e(f)$ from Equation (2) using the obtained $\Delta I(V)$. The absorption spectra of collective modes in high-T_c materials are localized near some frequencies, like shown in the hypothetical example on the bottom panel of Figure 2. So, it is also possible to make a simplified analysis of experimental data and point out the centers of the odd-symmetric features in the experimental dependences of the derivative $\mathrm{d}I/\mathrm{d}V$ vs. V (a green curve on the top panel of Figure 2) as the central frequencies of the modes.

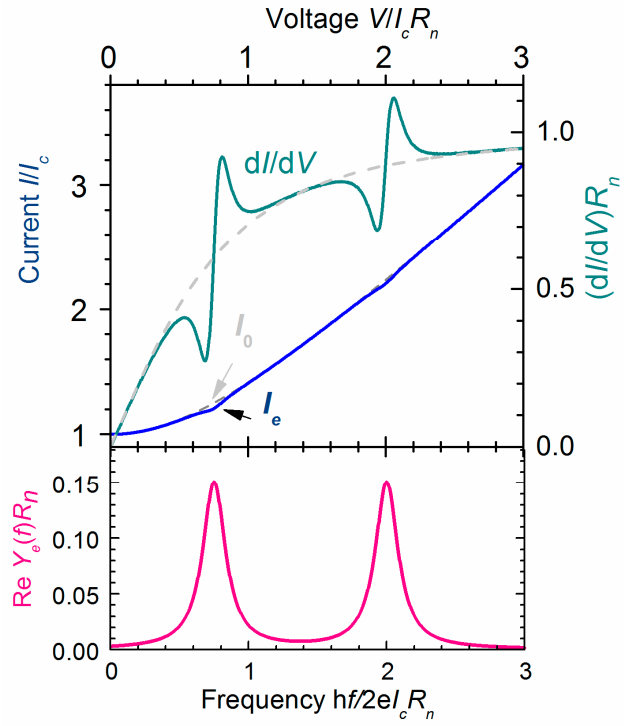

Figure 2. An example of the modification of the *I*–*V* curve of the Josephson junction described by the RSJ model (**top** panel) by a hypothetical external admittance containing two weak Lorentz lines at normalized frequencies $hf/2eI_cR_n = 0.75$ and 2 (**bottom** panel) in the real part. The spectral dependence of the external conductivity $Y_e(f)$ is related to the difference $\Delta I(V)$ between the modified I_e (solid blue) and autonomous I_0 (dashed grey) *I*–*V* curves according to Equation (2). A thick green curve is the first derivative dI/dV vs. voltage V of the junction under external shunting, while a dashed grey curve—dI_0/dV for the autonomous junction.

3. Results

The *I*–*V* curves of fabricated bicrystal $YBa_2Cu_3O_{7-x}$ junctions were measured in the current-bias mode using a four-probe technique. The differential resistances dV/dI have been measured by a current modulation technique with a lock-in amplifier, and differential conductances $dI/dV = (dV/dI)^{-1}$ have been calculated from the measured dV/dI. With current modulation not exceeding the thermal currents $I_{th} = 0.4$ μA at $T = 5$ K, it was possible to reach the accuracy $\delta(dI/dV)/dI/dV$ not worse than 1% at the amplifier bandwidth of 1 Hz. The voltage (and frequency) accuracy is finite due to voltage fluctuations, and the spectral resolution is due to the broadening of the Josephson linewidth by voltage fluctuations, correspondingly. The frequency accuracy of 1 GHz and spectral resolution of around 10 GHz are the typical values for JJ with R_n around 1 Ω [17].

Figure 3 shows the *I*–*V* curve and the dependence of the differential conductance dI/dV on the voltage V for typical bicrystal $YBa_2Cu_3O_{7-x}$ junctions fabricated from two *c*-axis thin films (a) and two films with mutually tilted *c*-axes (b). The data in Figure 3a belong to the JJ yd007201 on a 2 × 14° bicrystal $NdGaO_3$ substrate at $T = 5$ K. The data in Figure 3b correspond to the JJ yd502021 on a 2 × 12° bicrystal $SrTiO_3$ substrate at $T = 10$ K.

The *I*–*V* curve in Figure 3a is close to that in the RSJ model, with the resistance $R_n = 1.2$ Ω and the characteristic voltage $I_cR_n = 3$ mV (see the dashed line). The dependence of dI/dV vs. the voltage V for this sample shows no localized features and no noticeable deviations from the RSJ model. However, the *I*–*V* curve and the dependence of dI/dV vs. the voltage V for the JJ with mutually tilted *c*-axes (Figure 3b) demonstrate that there are noticeable deviations from the RSJ model, localized at voltages around 9.4 mV, as well as weaker deviations at voltages around 11.8 mV and 7.4 mV. There are also less intensive features at lower voltages. The noted features on the first derivatives of the *I*–*V* curves have an odd-symmetric form, which indicates

the localized dips in the *I–V* curve. Indeed, on the *I–V* curve in Figure 3, one can distinguish a dip at voltages of about 9.4 mV. The *I–V* curve in Figure 3b has been fitted to the RSJ model with the resistance R_n = 1.3 Ω and the characteristic voltage I_cR_n = 6 mV (see the dashed line).

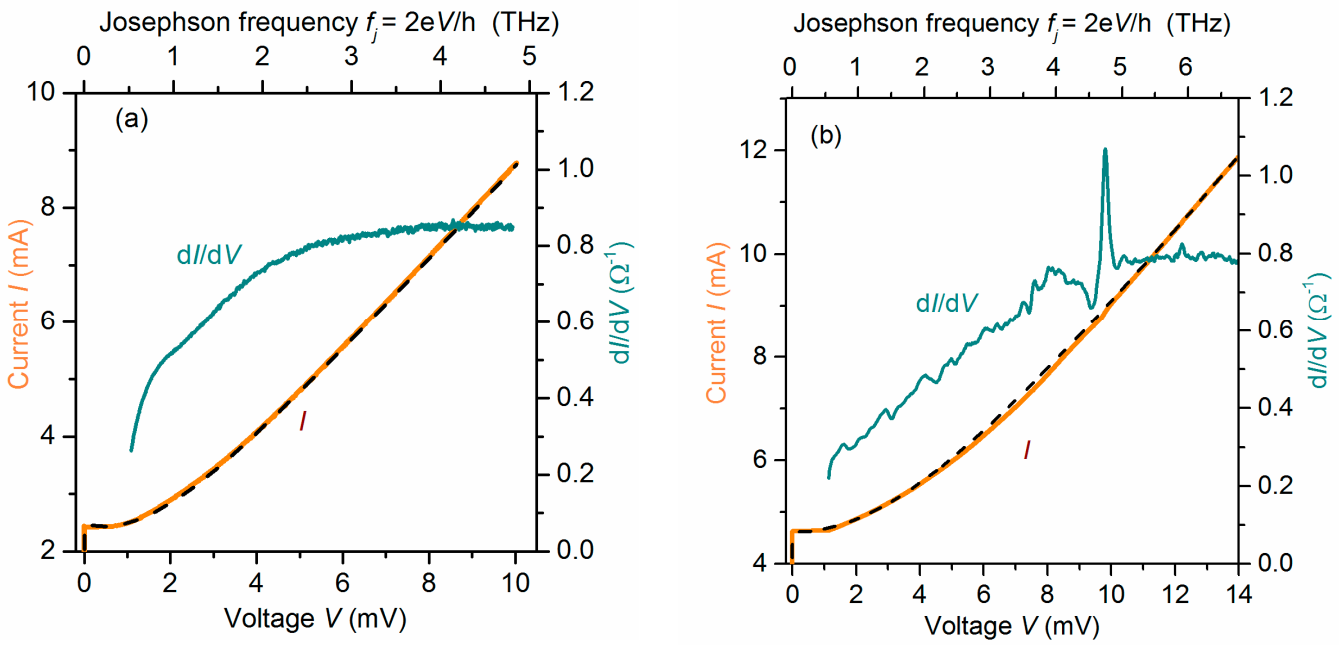

Figure 3. *I–V* curves and differential conductances d*I*/d*V* of typical bicrystal $YBa_2Cu_3O_{7-x}$ junctions formed from two *c*-axis thin films (**a**) and two films with mutually tilted *c*-axes (**b**) as a function of voltage *V* (bottom scale) and Josephson frequency f_j = 2e*V*/h (top scale). Dashed grey lines are fits to the *I–V* curves according to the RSJ model (Equation (1)).

The features on the *I–V* curves of $YBa_2Cu_3O_{7-x}$ bicrystal JJs with mutually tilted *c*-axes are reproducible in their positions on the voltage axis when fabricating JJs of various widths on various substrates ($SrTiO_3$ or $NdGaO_3$), and also at different temperatures. Figure 4 shows the dependences of the differential conductances for two JJs with different widths (a) and for one JJ at two temperatures (b). From Equation (2), it follows that the increase in losses $\mathrm{Re}Y_e(f)$ at some frequencies results in a local decrease of the current $\Delta I(V)$ through the JJ. If the loss function $\mathrm{Re}Y_e(f)$ has a Gaussian or Lorentzian form, then its mapping on the dependence of dI/dV on the voltage V should have an odd-symmetric form (see a green curve on the top panel of Figure 2). At low voltages, it deviates towards a smaller dI/dV, referring to the dependence dI_0/dV vs. V (a dashed grey curve on the top panel in Figure 2), and then, with increasing voltage—towards higher dI/dV. In this work, localized resonant features in dI/dV vs. V of odd symmetry, high reproducibility, and various intensities are of interest due to collective modes in high-*Tc* material of JJ. The extended features of low reproducibility and low intensity can be considered later.

Indeed, the upper curve in Figure 4a for the JJ with R_n = 0.8 Ω at voltages of about 9.4 mV has a well-defined feature that deviates at V < 9.4 mV towards lower conductances and at V > 9.4 mV—towards higher ones. In addition, the upper curve in Figure 4a has similar, but of low intensity, odd-symmetric features with centers at voltages V = 4.66 mV, 7.403 mV, 11.79 mV, and 11.98 mV (see also the enlarged features on the insets). The same features manifest in other JJs. Figure 4a also shows the dependence of dI/dV on voltage V for the JJ with R_n = 1.9 Ω (lower curve). The centers of the features on the upper curve in Figure 4a fit the centers of similar features on the lower curve. Moreover, the position of the singularities also remains unchanged with an increase in the JJ temperature. Figure 4b shows two dependences of dI/dV on voltage V for a JJ with R_n = 1.8 Ω at two temperatures of 5 K (lower curve) and 42 K (upper curve). It can be seen that all the main features retain their positions as the temperature rises by almost an order of magnitude.

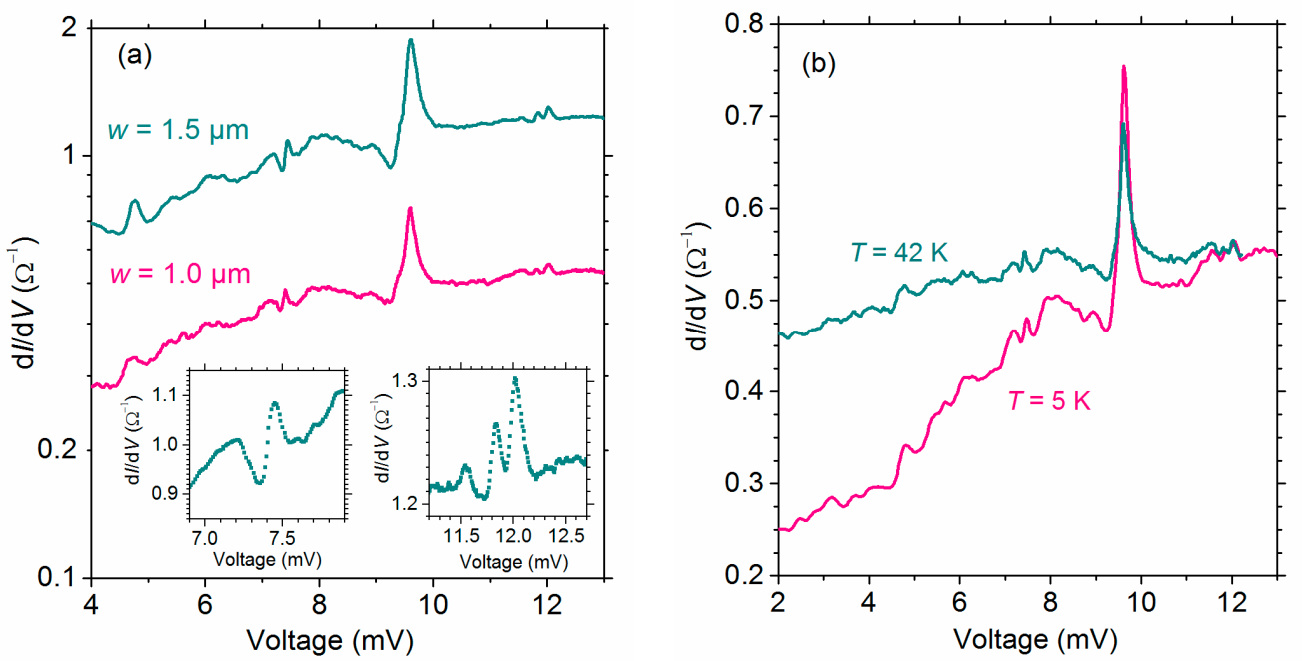

Figure 4. Dependences of differential conductivities dI/dV on voltage V: (**a**) for two JJs of different widths w at temperature T = 5 K, where the insets show enlarged features at 7.4 and 11.8 mV for the JJ with w = 1.5 μm; (**b**) for the JJ with w = 1 μm at T of 5 K and 42 K. Sample yd501282 on a 2 × 11.3° bicrystal $NdGaO_3$ substrate.

The features found on the I–V curves of $YBa_2Cu_3O_{7-x}$ bicrystal junctions with mutually tilted c-axes can be associated with both inelastic quasiparticle tunneling and Josephson tunneling. In the first case, the transformation of the voltages V_k of the features on the I–V curves of JJs into the position of the features on the frequency axis should occur according to the relation $V_k = hf_k/e$, while in the second case, $V_k = hf_k/2e$. To remove this uncertainty, we measured the I–V curves of JJs under irradiation with a frequency of 94 GHz and showed how the main feature on the I–V curves changed with the increasing power of this radiation.

The results are presented in Figure 5 for the dependence of the differential conductance dI/dV on the voltage V for one of the JJs. The unperturbed differential conductance dI/dV vs. V (red curve) has a peak at V = 9.6 mV. With a monotonous increase in radiation power, which corresponds to a decreasing the attenuation of a precision rotary-wave W10 attenuator from 60 dB to 4 dB, the dependence of dI/dV on the voltage V changes (see a corresponding set of curves with colors from red to purple). The main peak at 9.6 mV gradually fades to zero (blue curve) and reappears (navy and purple curve). In this case, additional local maxima show up, which are symmetrically situated from the main peak at V= 9.6 mV by ±194 μV (yellow curve). Then, the satellite peaks also appear at ± n × 194 μV with n = 2, 3, 4 (light blue, navy, and purple curves). The separation of these satellite peaks from each other and the main one is a multiple of 194 μV. This value is equal to the value hf/2e at a frequency f = 94 GHz, and not hf/e, as it could be if the cause of the formation of a feature in the I–V curve is the inelastic tunneling of quasiparticles [35].

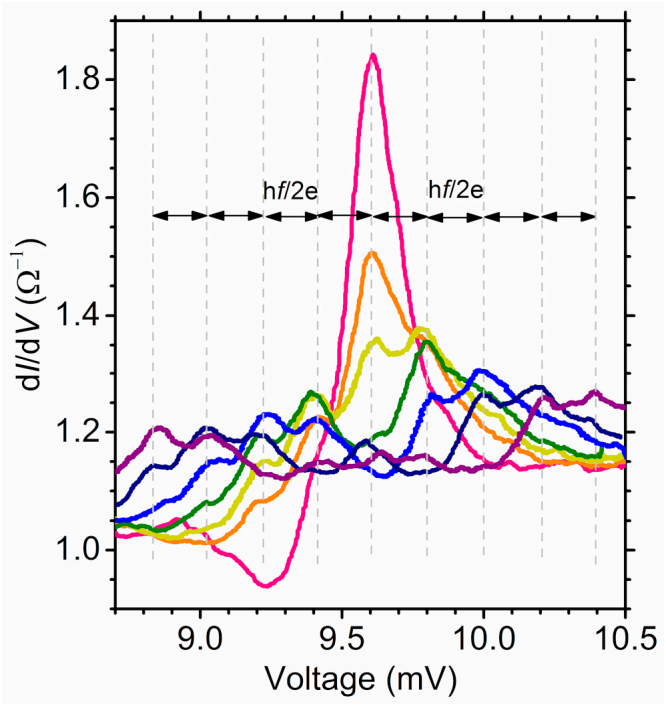

Figure 5. Modification of the differential conductance dI/dV on the voltage V of a JJ with mutually tilted c-axes (red curve) under electromagnetic irradiation with a frequency of f = 94 GHz with increasing power levels (curves from orange to purple). The vertical dashed lines are separated in voltage by $\pm$n $\times$ hf/2e = 194 μV (n = 1, 2, 3, 4) from the position of the peak at V = 9.6 mV on the unperturbed dI/dV versus V. Sample yd501282 on a 2 $\times$ 11.3° $NdGaO_3$ substrate. T = 5 K.

Thus, we can conclude that the features in the dc I–V curves of JJs are associated with the interaction of Josephson oscillations with frequency-localized modes in these JJs themselves and the nearest environment. The relative modulation of the differential conductance R_nΔdI/dV near the detected feature at voltages of about 9.4 mV reaches 80%, which means a significant mode intensity. The vibrational modes of separate organic molecules in tunneling barriers are usually weaker, with a relative conductance modulation of about 1% [28].

In connection with this circumstance, one should consider the frequencies of optical phonons or, more generally, collective modes in the JJ material itself, $YBa_2Cu_3O_{7-x}$. In this case, one should foresee that the oxygen concentration in the electrodes adjacent to the structural barrier of the JJ could decrease during the preparation of the JJ. This circumstance, in turn, can affect the position and shape of the features on the I–V curve of the JJ. To elucidate the effect of oxygen on the voltage position of features on the I–V curve, we measured several JJs as fabricated and after additional low-temperature annealing in atomic oxygen. Figure 6 presents the results, where the numbers on the curves correspond to the JJ numbers on the same substrate, and the letters "b" or "a" correspond to the junction state: b—before low-temperature annealing (before), a—after this annealing (after). As follows from Figure 6, annealing in atomic oxygen leads to a close to a twofold increase in the conductance $1/R_n$ of the JJs, an enhancement of the features around 9.4 mV and 4.7 mV, and a weakening of those at around 7.4 mV and 5.6 mV.

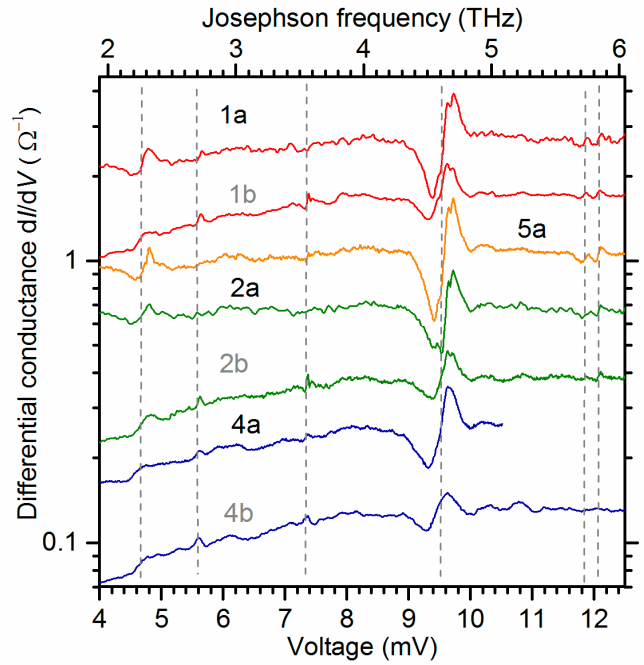

Figure 6. Differential conductances dI/dV vs. voltage V (bottom scale) and Josephson frequency $f_j = 2eV/h$ (top scale) for four JJs junctions of different widths on the same 2 × 11.3° bicrystal $NdGaO_3$ substrate with a 10 nm thick $SrTiO_3$ buffer layer. Sample yd705101_N, where N is the junction number on the substrate. The width values, in μm, are 6, 3, 2, and 1 for JJs, with numbers N of 1, 2, 5 and 4, correspondingly. The letter b means that the sample was measured before annealing, and the letter a means that the sample was measured after low-temperature annealing in atomic oxygen. T = 4.2 K.

The features at voltages 11.8 and 12 mV are weaker and increase slightly after annealing. The most intensive peculiarity at voltages near 9.4 mV has an internal structure that is noticeable even in unannealed samples (curves 1b, 2b). Two peaks are visible, the first at 9.55 mV and the second at 9.65 mV. Adding the oxygen content to the JJ increases the peak at 9.65 mV absolutely and relative to the peak at 9.55 mV (curves 1a, 2a).

4. Data Analysis and Discussion

Considering the intensity and reproducibility of the features on the *I–V* curves of $YBa_2Cu_3O_{7-x}$ JJs, one can suggest the involvement of the collective modes in $YBa_2Cu_3O_{7-x}$ in their formation. It makes sense to compare the features on the *I–V* curves of $YBa_2Cu_3O_{7-x}$ JJs with the results of far-infrared reflection experiments on bulk $YBa_2Cu_3O_{7-x}$ crystals. The intensity and position of some features in *I–V* curves changed after annealing; therefore, one should find the reference spectra for bulk samples $YBa_2Cu_3O_{7-x}$ with different oxygen contents x.

Table 1 summarizes the averaged values of the central frequencies f_k of the observed features on the *I–V* curves of bicrystal $YBa_2Cu_3O_{7-x}$ JJs (the first column) and compares these frequencies with the peak positions in the optical conductivity σ(f) of bulk crystals $YBa_2Cu_3O_{7-x}$ with different oxygen content, from $O_{6.0}$ (the second column) to $O_{6.95}$ (the sixth column). Data on optical conductivities σ(f) are from far-infrared reflection experiments [26–30] for two polarizations of the electric field E of incoming radiation: along the c-axis (E | | c) and along the a-axis (E | | a) of the $YBa_2Cu_3O_{7-x}$ crystals. If the f_k-values changed after annealing in atomic oxygen, two values $f_k^{(b)}$ and $f_k^{(a)}$ connected with the horizontal arrow. The vertical arrows ↑↓ indicate the increase (↑) or decrease (↓) of the intensities of the features after annealing.

Table 1. Central frequencies $f_k = 2eV_k/h$ of the features on the *I-V* curves of bicrystal $YBa_2Cu_3O_{7-x}$ JJs and the frequencies of the peaks in the optical conductivity of bulk crystals $YBa_2Cu_3O_{7-x}$ from far-infrared experiments [26–30]. The values $f_k{}^{(b)}$ are the average values for JJ before annealing in oxygen, while the values $f_k{}^{(a)}$ are the average values after annealing. All frequency values are in THz. The frequency values in bold correspond to the most intensive lines.

Our Data $YBa_2Cu_3O_{7-x}$ JJ fk(b) → fk(a); ↓ ↑	[27,29] $YBa_2Cu_3O_{6.0}$ E ⫽ c E ⫽ a	[26,30] $YBa_2Cu_3O_{6.5}$ E ⫽ c E ⫽ a	[26] $YBa_2Cu_3O_{6.7}$ E ⫽ c	[26] $YBa_2Cu_3O_{6.85}$ E ⫽ c	[26,29] $YBa_2Cu_3O_{6.95}$ E ⫽ c E ⫽ a
2.24 → 2.27; ↑					
2.69; ↓		2.79			
3.54; ↓	3.48	3.39			
		3.75			
	4.38	**4.35**	4.08		
			4.41	4.41	
			4.59	**4.59**	
4.59 → 4.62; ↑					**4.65**
		4.83			
5.71; ↑	5.64	5.70			5.69
5.81; ↑			5.67	5.76	5.82

The most intensive feature on the *I–V* curves of JJs is observed at $f_k{}^{(b)}$ = 4.59 THz. It shifts to a higher frequency of $f_k{}^{(a)}$ = 4.62 THz after annealing in oxygen with the intensity increase (↑). These frequency values are close to the corresponding values for the intensive collective modes observed in the reflection spectra of $YBa_2Cu_3O_{6.85}$ and $YBa_2Cu_3O_{6.95}$ [26] when the electric field E of radiation is parallel to the c-axis of the crystals. The highly doped $YBa_2Cu_3O_{6.95}$ material contains an intensive optical phonon mode at 4.65 THz (the sixth column), which splits into two modes at 4.59 THz and 4.41 THz in $YBa_2Cu_3O_{6.85}$ with reduced oxygen content (the fifth column). The 4.59 THz mode is more intensive than the mode at 4.41 THz in $YBa_2Cu_3O_{6.85}$, but with further oxygen reduction, the 4.41 THz mode dominates in $YBa_2Cu_3O_{6.7}$ (the fourth column), and additional splitting appears at 4.08 THz. Thus, the observed frequency shift (4.59 THz to 4.62 THz) in the feature on the *I–V* curve after annealing can be ascribed to the transformation of some parts of the $YBa_2Cu_3O_{7-x}$ material near the bicrystal boundary from $YBa_2Cu_3O_{6.85}$ to near $YBa_2Cu_3O_{6.95}$.

The less intensive 5.81 THz feature on the *I–V* curves corresponds to the optical phonon mode at 5.82 THz in reflection measurements with E ⫽ c for $YBa_2Cu_3O_{6.95}$. However, it does not depend on oxygen deficiency, as follows from reflection measurements. The 5.71 THz feature on the *I–V* curves seems to belong to the 5.69 THz mode in reflection measurements with E ⫽ a for $YBa_2Cu_3O_{6.95}$, which does not change when going from $YBa_2Cu_3O_{6.95}$ to $YBa_2Cu_3O_{6.5}$. The intensities of the features at 2.69 and 3.54 THz on the *I–V* curves of JJs decrease with annealing in oxygen. Therefore, the collective modes in the bulk $YBa_2Cu_3O_{7-x}$ with low oxygen content can be responsible for these features. Indeed, there are the modes at 2.79 THz in $YBa_2Cu_3O_{6.5}$ at E ⫽ c and at 3.48 THz in $YBa_2Cu_3O_{6.0}$ at E ⫽ a (the third and second columns in Table 1). Moreover, there are no modes with close frequencies in $YBa_2Cu_3O_{7-x}$ with higher oxygen content.

The second-strongest feature on the *I–V* curves, with frequency transformation from 2.24 to 2.27 THz after annealing, has no candidate among the collective modes in $YBa_2Cu_3O_{7-x}$ crystals. It looks like a replica of the 4.6 THz feature but at approximately twice as low frequencies. In weak perturbation of RSJ-like dynamics by external admittances of low values $|Y_e(f_c)| << {R_n}^{-1}$ (see Equation (2)), a contribution to the *I–V* curve comes only from the first Josephson harmonic at the frequency $f = 2eV/h$. However, the current-phase relation in the real JJ can contain the sin2φ-term, $I_s = I_{c1}\mathrm{Sin}\varphi + I_{c2}\mathrm{Sin}2\varphi$, and the *I–V* curve can demonstrate an additional feature at

voltages V around $(1/2)hf_k/2e$. In this case, the I-V curve of JJ should demonstrate a subharmonic resonance at $V = (1/2)hf/2e$ on the I–V curves under weak THz irradiation. However, the experiments with similar bicrystal JJs and frequencies f of several THz did not reveal these subharmonic features [36]. In addition, from a theoretical point of view, bicrystal $YBa_2Cu_3O_{7-x}$ JJs with the mutually tilted c-axes are similar to so-called d0-d0 junctions and should have a pure $\sin\varphi$-dependence of the current I_s vs. the phase difference φ [37]. Due to these experimental and theoretical grounds, we cannot consider this explanation of the subharmonic feature on the I–V curves by the $\sin 2\varphi$-term as a dominant one.

Staying inside the RSJ model, one more explanation can be related to more intensive external shunting by $|Y_e(f_c)|$ comparable with ${R_n}^{-1}$. In this case, the interaction of the second Josephson harmonic at the frequency $f = 2 \times 2eV/h$ with the collective modes at frequencies f_k around 4.6 THz can give the feature at V around $(1/2)hf_k/2e$. To quantify this effect, one can either analytically consider the perturbation of RSJ dynamics by shunting in the second-order approximation, $\sim(|Y_e(f_c)|\ R_n)^2$, or make numerical simulations for various values of $|Y_e(f_c)|\ R_n$.

One can suggest that bicrystal junctions formed from two mutually tilted c-axis films can have inhomogeneous currents along the boundary with several dominating channels and behave as a superconducting interferometer with dynamics different from those of a single RSJ-like JJ [38]. Even for two JJs in the interferometer, the appearance of the subharmonic Shapiro steps is predicted [39]. An additional subharmonic feature at $V = (1/2)hf/2e$ was on the 1 THz detector response of the c-axis bicrystal junction JJ of 8 μm width but absent in a similar junction of 2.5 μm width [20]. However, the appearance of the subharmonic features in the JJ with mutually tilted c-axes does not depend on the width of the JJ, as one can see from Fig. 6, where subharmonic features are the same for 6 μm(N1) and 1 μm(N4) junctions. Therefore, we can conclude that interferometric effects on Josephson dynamics of the JJs cannot be the only reason for the features at V around $(1/2)hf_k/2e$.

Nonlinear effects in $YBa_2Cu_3O_{7-x}$ material itself under an intensive THz electric field from Josephson oscillations can be an alternative option to clarify the nature of the subharmonic feature at V around $(1/2)hf_k/2e$ on the I–V curves of $YBa_2Cu_3O_{7-x}$ bicrystal JJs. THz emission due to a nonlinear optical rectification (OR) in $YBa_2Cu_3O_{7-x}$ has already been observed [40]. One can expect that a second harmonic generation (SHG) in this material because the OR and SHG processes result from the same nonlinearity in optical materials [41]. There are no data on the effective nonlinear susceptibilities for OR and SHG in $YBa_2Cu_3O_{7-x}$; however, the electric THz fields from Josephson oscillations are rather intensive. Estimates give the field values around 5×10^4 V/cm for the voltages near the subharmonic feature on the I–V curves. A detailed consideration of these effects deserves a separate publication.

The differences between the frequencies of collective modes detected by Josephson spectroscopy in $YBa_2Cu_3O_{7-x}$ thin-film JJs and by reflection measurements of bulk $YBa_2Cu_3O_{7-x}$ crystals can exist, because the $YBa_2Cu_3O_{7-x}$ thin films are under considerable strain due to the differences in lattice constants and thermal expansion coefficients with the substrates. However, data comparison from Josephson and reflection spectroscopies shows that differences in the recovered frequency values are low. This circumstance stimulates further development of Josephson spectroscopy for studying collective modes in JJs and their environment.

As a first step in this direction, the admittances $\mathrm{Re}Y(f)$ near the intensive mode at around 4.6 THz were recovered from the experimental curves dI/dV vs. V according to the procedure described in Section 2.2. Figure 7a shows the recovered $\mathrm{Re}Y(f)$ of the JJ (1a in Figure 6) after low-temperature annealing in atomic oxygen, while Figure 7b shows that before annealing (1b in Figure 6). The maximal value of the admittance $\mathrm{Re}Y(f)$ after annealing is twice as high as the same value before annealing. The forms of these absorption lines are asymmetric and different.

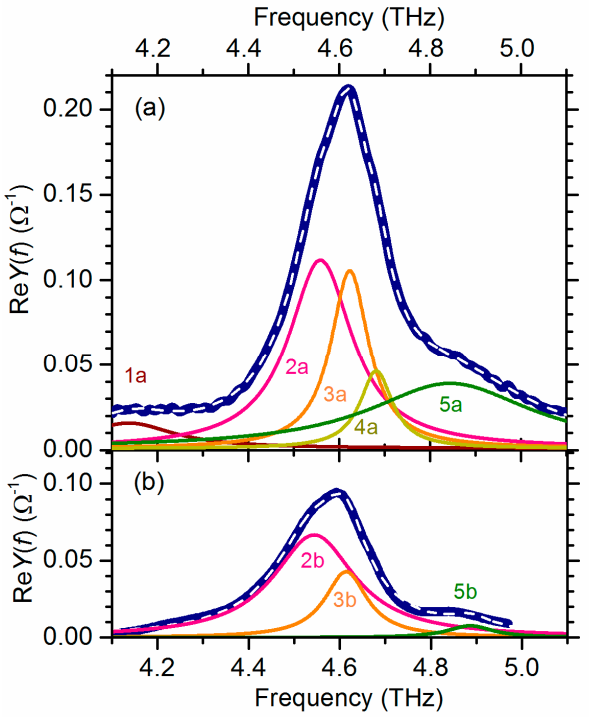

Figure 7. Real parts of dynamic conductances Re$Y(f)$ for JJ yd705101_1 (thick navy lines) recovered from experimental data in Figure 6 according to Josephson admittance spectroscopy: (**a**) after low-temperature annealing in atomic oxygen, (**b**) before annealing. Dashed grey lines are nonlinear fits by multiple Lorentz curves. The thin colored lines are Lorentz curves from the fits. Parameters are in the text.

The optical phonon lines in bulk crystals $YBa_2Cu_3O_{7-x}$ determined by Fourier spectroscopy are usually close to Lorentz curves. However, each of the recovered Re$Y(f)$ curves in Figure 7 is more complicated than a single Lorentzian. The form of the spectrum Re$Y(f)$ (a thick line after annealing (Figure 7a)) fits well with five Lorentz curves with the following central frequencies f_{ka} and the linewidths δf_{ka}, in THz: $f_{1a} = 4.14$, $\delta f_{1a} = 0.245$; $f_{2a} = 4.56$, $\delta f_{2a} = 0.171$; $f_{3a} = 4.62$, $\delta f_{3a} = 0.102$; $f_{4a} = 4.68$, $\delta f_{4a} = 0.087$; $f_{5a} = 4.84$, $\delta f_{5a} = 0.43$. A sum of three Lorentz curves is sufficient to fit the spectrum Re$Y(f)$ (thick navy curve in Figure 7b) for the same JJ before annealing in oxygen. The fit parameters, in THz, are the following: $f_{2b} = 4.54$, $\delta f_{2b} = 0.219$; $f_{3b} = 4.61$; $\delta f_{3b} = 0.113$; $f_{5b} = 4.89$, $\delta f_{5b} = 0.12$. Comparison of the results of nonlinear fits for the same JJ before and after annealing shows that three spectral components at $f_2 = (4.55 \pm 0.01)$ THz; $f_3 = (4.61 \pm 0.01)$ THz and $f_5 = (4.86 \pm 0.03)$ THz practically did not change the positions of their maxima, but increased their peak values by about two, three and four times, correspondingly.

In addition, two extra Lorentz curves appeared at $f_1 = 4.14$ THz and $f_4 = 4.68$ THz after annealing, while the curve at 4.68 THz has a narrow linewidth of around 0.09 THz. This low linewidth is a hint that the mode at $f_4 = 4.68$ THz belongs to highly oxygenated $YBa_2Cu_3O_{7-x}$ [26]. The general trend in the constituent Lorentzians in the spectra in Figure 7a,b is the intensification of the lines at f_2, f_3, and f_5 and the appearance of new lines at f_1 and f_4 in the spectral range from 4.1 THz to 5.1 THz. This trend is in qualitative agreement with the tendency deduced from the data in Table 1 (see also [26]), where initial deoxygenation results in the splitting of the 4.65 THz line, followed by an increase in the number of splitted lines and frequency differences in splitting with further deoxygenation.

It is worthwhile to compare quantitatively the absorption lines obtained by Josephson admittance spectroscopy lines in the $YBa_2Cu_3O_{7-x}$ bicrystal thin-film JJ and those in the reflection spectra of $YBa_2Cu_3O_{7-x}$ single crystals [26]. The narrowest line at $f_4 = 4.68$ THz in the $YBa_2Cu_3O_{7-x}$ JJ can be from the optical phonon mode with $E \mid\mid c$, observed in $YBa_2Cu_3O_{6.95}$ single crystals at 4.65 THz. The lines at $f_3 = 4.62$ THz, $f_2 = 4.56$ THz,

and f_1 = 4.14 THz can be from the splitted collective modes at 4.59 THz, 4.41 THz, and 4.08 THz in $YBa_2Cu_3O_{6.7}$. The line at f_5 = 4.84 THz in the $YBa_2Cu_3O_{7-x}$ JJ can be due to the splitted collective mode at 4.83 THz in $YBa_2Cu_3O_{6.5}$. This comparison makes it possible to estimate the oxygen distribution in $YBa_2Cu_3O_{7-x}$ near the bicrystal boundary of JJs made from $YBa_2Cu_3O_{7-x}$ thin films with mutually tilted *c*-axes.

After this comparison, one can suggest some mixed composition, from $YBa_2Cu_3O_6$ (with no oxygen in the chains) to $YBa_2Cu_3O_{6.85}$ (the chains partly filled with oxygen), in the $YBa_2Cu_3O_{7-x}$ electrodes of the bicrystal JJ as fabricated. After annealing in atomic oxygen, this composition changes to the mixture of $YBa_2Cu_3O_{6.5}$ (Ortho II phase, with a double unit cell normal to the chain direction) and $YBa_2Cu_3O_{6.95}$ (close to $YBa_2Cu_3O_7$, fully oxygenated Ortho I phase). So, $YBa_2Cu_3O_{7-x}$ electrodes near the bicrystal boundary in the JJs under study have parts with slightly different and relatively low oxygen content, and annealing increases the average oxygen content but does not reach the maximum oxygenation. Presumably, more intensive and longer treatment of JJs in atomic oxygen should be developed.

5. Conclusions

Thus, the features in the *I–V* curves of bicrystal Josephson junctions made from $YBa_2Cu_3O_{7-x}$ films with mutually tilted *c*-axes are due to the interaction of Josephson oscillations with the collective modes in the $YBa_2Cu_3O_{7-x}$ material adjacent to the bicrystal boundary. A change in the oxygen concentration in the Cu-O chains in $YBa_2Cu_3O_{7-x}$ leads to a change in the composition of the collective modes and, accordingly, to the appearance or disappearance of features in the *I–V* curves of the JJs. These circumstances have a significant effect on the absorption spectrum of these JJs and can limit their use in spectroscopic applications. According to our data, losses in the THz frequency range from 2.5 THz up to 4 THz are lower in $YBa_2Cu_3O_{7-x}$ JJs after additional loading with oxygen. Therefore, optimization of annealing in atomic oxygen appears to be a necessary final part of the fabrication technology of high-quality $YBa_2Cu_3O_{7-x}$ JJs for THz applications. This work paves the way towards probing collective modes in high-T_c materials in situ using Josephson admittance spectroscopy.

Funding: This research received no external funding.

Institutional Review Board Statement: Not applicable.

Informed Consent Statement: Not applicable.

Data Availability Statement: Not applicable.

Acknowledgments: The author is thankful to U. Poppe for the deposition of a thin buffer layer of $SrTiO_3$ on the $NdGaO_3$ bicrystal substrate used for fabrication of the sample yd705101.

Conflicts of Interest: The author declares no conflict of interest.

References

1. Bednorz, J.G.; Muller, K.A. Possible high-T_c superconductivity in the Ba–La–Cu–O system. *Z. Phys. B* **1986**, *64*, 189–193. [CrossRef]
2. Josephson, B.D. Possible new effects in superconductive tunneling. *Phys. Lett.* **1962**, *1*, 251–253. [CrossRef]
3. Hilgenkamp, H.; Mannhart, J. Grain boundaries in high-T_c superconductors. *Rev. Mod. Phys.* **2002**, *74*, 485–549. [CrossRef]
4. Likharev, K.K. *Dynamics of Josephson Junctions and Circuits*; Gordon and Breach: New York, NY, USA, 1986.
5. Divin, Y.Y. Detection and Spectroscopy of Electromagnetic Radiation by Josephson Junctions from High-Temperature Superconductors. Doctor Thesis, Kotelnikov Institute of Radioengineering and Electronics of Russian Academy of Sciences, Moscow, Russia, 2011.
6. Divin, Y.; Snezhko, A.; Poppe, U.; Gundareva, I.; Pavlovskiy, V. Screening of Liquids with Quasioptical High-T_c Josephson Detectors. In *Nanotechnology in the Security Systems (NATO Science for Peace and Security Series C: Environmental Security)*; Bonča, J., Kruchinin, S., Eds.; Springer: Dordrecht, The Netherlands, 2015; Part II; pp. 165–179.
7. Kume, E.; Iguchi, I.; Takahashi, H. On-chip spectroscopic detection of terahertz radiation emitted from a quasiparticle-injected nonequilibrium superconductor using a high-T_c Josephson junction. *Appl. Phys. Lett.* **1999**, *75*, 2809–2811. [CrossRef]
8. Kaneko, R.; Kawayama, I.; Murakami, H.; Tonouchi, M. Detection of pulsed terahertz waves using high-temperature superconductor Josephson junction. *Appl. Phys. Express* **2010**, *3*, 042701. [CrossRef]

9. An, D.Y.; Yuan, J.; Kinev, N.; Li, M.Y.; Huang, Y.; Ji, M.; Zhang, H.; Sun, Z.L.; Kang, L.; Jin, B.B.; et al. Terahertz emission and detection both based on high-*Tc* superconductors: Towards an integrated receiver. *Appl. Phys. Lett.* **2013**, *102*, 092601. [CrossRef]
10. Divin, Y.Y.; Poppe, U.; Urban, K.; Volkov, O.Y.; Shirotov, V.V.; Pavlovskii, V.V.; Schmueser, P.; Hanke, K.; Geitz, M.; Tonutti, M. Hilbert-transform spectroscopy with high-T_c Josephson junctions: First spectrometers and first applications. *IEEE Trans. Appl. Supercond.* **1999**, *9*, 3346–3349. [CrossRef]
11. Divin, Y.; Pandya, H.K.B. Feasibility of ECE measurements using Hilbert-transform spectral analysis. *Fusion Sci. Technol.* **2014**, *65*, 399–405. [CrossRef]
12. Divin, Y.Y.; Schulz, H.; Poppe, U.; Klein, N.; Urban, K.; Pavlovskii, V.V. Millimeter-wave Hilbert-transform spectroscopy with high-*Tc* Josephson junctions. *Appl. Phys. Lett.* **1996**, *68*, 1561–1563. [CrossRef]
13. Divin, Y.Y.; Liatti, M.V.; Shirotov, V.V.; Poppe, U.; Gubankov, V.N.; Urban, K. Terahertz Josephson detectors and Hilbert spectroscopy. In Proceedings of the Infrared and Millimeter Waves, Conference Digest of the 2004 Joint 29th International Conference on 2004 and 12th International Conference on Terahertz Electronics, Karlsruhe, Germany, 27 September–1 October 2004; Thumm, M., Wiesbeck, W., Eds.; IEEE: Piscataway, NJ, USA; pp. 277–278.
14. Xu, W.W.; Chen, J.; Kang, L.; Wu, P.H. Extraction of the spectral information of terahertz signals using superconducting Josephson junction. *Sci. China Technol. Sci.* **2010**, *53*, 1247–1251. [CrossRef]
15. Divin, Y.; Snezhko, A.; Lyatti, M.; Poppe, U.; Pavlovskiy, V. Terahertz Applications of Hilbert-Transform Spectral Analysis. *IEEE Trans. Appl. Supercond.* **2014**, *24*, 1500807. [CrossRef]
16. Snezhko, A.V.; Gundareva, I.I.; Lyatti, M.V.; Volkov, O.Y.; Pavlovskiy, V.V.; Poppe, U.; Divin, Y.Y. Terahertz Josephson spectral analysis and its applications. *Supercond. Sci. Technol.* **2017**, *30*, 044001. [CrossRef]
17. Volkov, O.; Pavlovskiy, V.; Gundareva, I.; Khabibullin, R.; Divin, Y. *In Situ* Hilbert-Transform Spectral Analysis of Pulsed Terahertz Radiation of Quantum Cascade Lasers by High-T_c Josephson. *IEEE Trans. Terahertz Sci. Technol.* **2021**, *11*, 330–338. [CrossRef]
18. Volkov, O.; Pavlovskiy, V.; Divin, Y. Application of High-T_c Josephson Detectors for Spectral Characterization of THz Quantum Cascade Lasers. *IEEE Trans. Appl. Supercond.* **2022**, *32*, 2300105. [CrossRef]
19. Volkov, O.Y.; Duzhikov, I.N.; Khabibullin, R.A.; Baranov, A.N.; Divin, Y.Y. Subterahertz difference-frequency generation in terahertz quantum cascade lasers. *Appl. Phys. Lett.* **2022**, *121*, 263504. [CrossRef]
20. Divin, Y.Y.; Kotelyanskii, I.M.; Gubankov, V.N. Bicrystal Josephson Junctions for Terahertz Hilbert-Transform Spectroscopy. *J. Commun. Technol. Electron.* **2003**, *48*, 1137–1147.
21. Divin, Y.Y.; Poppe, U.; Jia, C.L.; Shadrin, P.M.; Urban, K. Structural and electrical properties of $YBa_2Cu_3O_{7-x}$ [100]-tilt grain boundary Josephson junctions with large I_cR_n-product on $SrTiO_3$ bicrystals. *Phys. C* **2002**, *372*, 115–118. [CrossRef]
22. Gundareva, I.; Divin, Y. YBa2Cu3O7-x bicrystal Josephson junctions with high IcRn-products and wide-ranging resistances for THz applications. *IEEE Trans. Appl. Supercond.* **2016**, *26*, 1100204. [CrossRef]
23. Humlíček, J.; Litvinchuk, A.P.; Kress, W.; Lederle, B.; Thomsen, C.; Cardona, M.; Habermeier, H.-U.; Trofimov, I.; König, W. Lattice vibrations of $Y_{1-x}Pr_xBa_2Cu_30_7$: Theory and experiment. *Phys. C* **1993**, *206*, 345–359. [CrossRef]
24. Grüninger, M.; Van der Marel, D.; Tsvetkov, A.A.; Erb, A. Observation of Out-of-Phase Bilayer Plasmons in $YBa_2Cu_3O_{7-\delta}$. *Phys. Rev. Lett.* **2000**, *84*, 1575–1578. [CrossRef]
25. Genzel, L. Far-Infrared Fourier Transform Spectroscopy. In *Millimeter and Submillimeter Wave Spectroscopy of Solids*; Grüner, G., Ed.; Springer: Berlin/Heidelberg, Germany, 1998; Chapter 5.
26. Homes, C.C.; Timusk, T.; Bonn, D.A.; Liang, R.; Hardy, W.N. Optical phonons polarized along the c-axis of $YBa_2Cu_3O_{6+x}$, for x = 0.5→0.95. *Can. J. Phys.* **1995**, *73*, 663–675. [CrossRef]
27. Bauer, M.; Ferreira, I.B.; Genzel, L.; Cardona, M.; Murugaraj, P.; Maier, J. Far-Infrared Study of Optical Phonons in an $YBa_2Cu_3O_6$ Crystal. *Solid State Commun.* **1989**, *72*, 551–554. [CrossRef]
28. Tajima, S.; Ido, T.; Ishibashi, S.; Itoh, T.; Eisaki, H.; Mizuo, Y.; Arima, T.; Takagi, H.; Uchida, S. Optical-phonon study of single crystals of various layered cuprates and related materials: Evidence of unique electron-phonon coupling in the CuO_2 plane. *Phys. Rev. B* **1991**, *43*, 10496–10507. [CrossRef]
29. Bernhard, C.; Holden, T.; Humlıcek, J.; Munzar, D.; Golnik, A.; Kläser, M.; Wolf, T.; Carr, L.; Homes, C.; Keimer, B. In-plane polarized collective modes in detwinned $YBa_2Cu_3O_{6.95}$ observed by spectral ellipsometry. *Solid State Commun.* **2002**, *121*, 93–97. [CrossRef]
30. Hwang, J.; Yang, J.; Timusk, T.; Sharapov, S.G.; Carbotte, J.P.; Bonn, D.A.; Liang, R.; Hardy, W.N. *a*-axes optical conductivity of detwinned ortho-II $YBa_2Cu_3O_{6.50}$. *Phys. Rev. B* **2006**, *73*, 014508. [CrossRef]
31. Liatti, M.V.; Poppe, U.; Divin, Y.Y. Low-frequency voltage noise and electrical transport in [100]-tilt $YBa_2Cu_3O_{7-x}$ grain-boundary junctions. *Appl. Phys. Lett.* **2006**, *88*, 152504. [CrossRef]
32. Conder, K. Oxygen diffusion in the superconductors of the YBaCuO family: Isotope exchange measurements and models. *Mater. Sci. Eng.* **2001**, *R32*, 41–102. [CrossRef]
33. Volkov, A.F. Effect of external impedance on dc *I-V* curve of Josephson junction. *Radio Eng. Electron. Phys.* **1972**, *17*, 2068–2070.
34. McCumber, E. Effect of ac Impedance on dc Voltage-Current Characteristics of Superconductor Weak-Link Junctions. *J. Appl. Phys.* **1968**, *39*, 3113–3118. [CrossRef]
35. Wolf, E.L. *Principles of Electron Tunneling Spectroscopy*; Oxford University Press: New York, NY, USA, 1985.
36. Divin, Y.Y.; Tkachev, D.A.; Pavlovskii, V.V.; Volkov, O.Y.; Liatti, M.V.; Gubankov, V.N.; Urban, K. Classical and Josephson detection of terahertz radiation using $YBa_2Cu_3O_{7-x}$ [100]-tilt bicrystal junctions. *J. Phys. Conf. Ser.* **2006**, *43*, 1322–1325. [CrossRef]

37. Kawabata, S.; Kashiway, S.; Asano, Y.; Tanaka, Y.; Kato, T.; Golubov, A.A. Theory of macroscopic quantum tunnelling and dissipation in high-*T*c Josephson junctions. *Supercond. Sci. Technol.* **2007**, *20*, S6–S9. [CrossRef]
38. Fillipov, A.T.; Gal'pern, Y.S. Bound states, bifurcations and static chaos in Josephson lattices. *Phys. Lett. A* **1993**, *172*, 471–474. [CrossRef]
39. Kornev, V.K.; Arzumanov, A.V.; Constantinian, K.Y.; Mashtakov, A.D.; Ovsyannikov, G.A. Spectral study of the Shapiro subharmonic step formation. *Appl. Supercond.* **1997**, *158*, 559–562.
40. Siders, J.L.W.; Trugman, S.A.; Garzon, F.H.; Houlton, R.J.; Taylor, A.J. Terahertz emission from $YBa_2Cu_3O_{7-\delta}$ thin films via bulk electric-quadrupole–magnetic-dipole optical rectification. *Phys. Rev. B* **2000**, *61*, 13633–13638. [CrossRef]
41. Boyd, R.W. *Nonlinear Optics*; Academic Press: London, UK, 2008.